ON THE SIGNIFICANCE OF THE HIGHER ORDER STRESS IN RISER VIV RESPONSES

Jie Wu
SINTEF Ocean
Otto Nielsen veg 10, 7052
Trondheim, Norway
Jie.Wu@SINTEF.NO

Decao Yin
SINTEF Ocean
Otto Nielsen veg 10, 7052
Trondheim, Norway
Decao.yin@sintef.no

Halvor Lie
SINTEF Ocean
Otto Nielsen veg 10, 7052
Trondheim, Norway
Lie.Halvor@sintef.no

Carl M. Larsen
NTNU
Otto Nielsen veg 10, 7052
Trondheim, Norway
carl.m.larsen@ntnu.no

Rolf J. Baarholm
Equinor
Strandvegen 4, 7500
Stjørdal, Norway
rolbaa@equinor.com

Stergios Liapis
Shell International Exploration and Production Inc.
3333 Highway 6 South - Mg
148. Houston, TX 77210, Texas, USA
liapis101@gmail.com

ABSTRACT

Vortex-Induced Vibrations (VIV) can lead to fast accumulation of fatigue damage and increased drag loads for slender marine structures. VIV responses mainly occur at the vortex shedding frequency, while higher harmonics can also be excited. Recent VIV model tests with flexible pipes have shown that higher harmonics in cross-flow (CF) direction can contribute to the fatigue damage significantly due to its higher frequency. Rigid cylinder experiments shown that the CF 3rd order harmonics are more pronounced when the motion orbit is close to a 'figure 8' shape and the cylinder is moving against the flow at its largest CF motion. However, there is still lack of understanding of when and where higher harmonics occur for a flexible pipe. Therefore, significant uncertainty remains on how to account for fatigue damage due to higher harmonics in VIV prediction.

In the present paper, representative VIV data from various riser model test campaigns are carefully studied and analyzed. The key parameters that influence the magnitude of the 3rd order harmonic stress are found to be the bending stiffness, the reduced velocity and the orbit stability. The experimental data is analyzed in order to assess the impact of each parameter on the 3rd order harmonic stress. A preliminary empirical response model to estimate the maximum CF 3rd order harmonic stress based on these identified structural and hydrodynamic parameters has been proposed. The results of this study will contribute to reduce the uncertainty and un-necessary conservatism in VIV prediction.

NOMENCLATURE

b	Subscript, short for beam
CF	Cross-flow
IL	In-line
NDP	Norwegian Deepwater Programme
s	Subscript, short for string
Shear7	VIV prediction software developed by Prof. Vandiver's group
VIV	Vortex-induced vibration
VIVA	VIV prediction software developed by Prof. Triantafyllou's group
VIVANA	VIV prediction software developed by Prof. Larsen's group
A	Displacement amplitude
A/D	Displacement amplitude ratio
D	Diameter of the cylinder
f	Frequency
$f_{CF,dom}$	Dominating response frequency in cross-flow direction
f_n	Natural frequency of a rigid cylinder on elastic supports
$f_{n,b}$	Natural frequency of a un-tensioned beam
$f_{n,s}$	Natural frequency of a tensioned string
$f_{n,tot}$	Natural frequency of a tensioned beam
f_{St}	Strouhal frequency
f_{osc}	Response frequency a tensioned beam
$\hat{f}$	Non-dimensional frequency $\hat{f} = f_{osc}D/U$
C_s	Theoretical travelling speed of a tensioned string (m/s)
$C_{b,IL/CF}$	Theoretical travelling speed of a beam (m/s)
$C_{IL/CF}$	Measured IL/CF travelling speed (m/s)
EI	Bending stiffness (N/m^2)
L	Length of the pipe

m	Mass per unit length, including added mass coefficient of 1.0 (kg/m)
n	Mode number
$N_{CF,dom}$	Dominating response mode in cross-flow direction
R	Outer radius of the cross section of the pipe
St	Strouhal number
T	Tension (N)
t	Time
U	Current speed
U_{max}	Maximum towing speed of a sheared flow test
Ur	True reduced velocity $U_r = U/(Df_{osc})$
V_{rn}	Reduced velocity of a rigid cylinder on elastic supports $V_{rn} = U/(Df_n)$
w_n	Model weight of n^{th} mode
x	IL displacement (m)
y	CF displacement (m)
z	Coordinate along the pipe
X	IL displacement amplitude (m)
Y	CF displacement amplitude (m)
Δt	Time difference between the CF and IL displacement zero up-crossings
ζ	Damping ratio
θ	Motion phase angle (deg)
κ	Curvature
ε	Strain
φ_n	N^{th} mode shape
ω	Circular frequency (rad/s)

1 INTRODUCTION

When a cylinder is subjected to an incoming flow, vortices are shed from both sides of the cylinder. The vortex shedding will lead to periodic hydrodynamic forces which cause the cylinder to oscillate in both in-line (IL) and CF directions. This phenomenon is called Vortex Induced Vibrations (VIV). VIV can lead to fast accumulation of fatigue damage as well as increased drag loads on slender marine structures. Therefore, it should be considered during design phase on deep water riser systems.

Depending on the test models, VIV experiments could be categorized as flexible pipe VIV tests and rigid cylinder VIV tests. Representative flexible VIV tests are Norwegian Deepwater Programme (NDP) high mode VIV test [1], Shell 38m VIV test [2], the ExxonMobil rotating rig test [3],[4] and the Hanøytangen test [5]. In these tests, bending strain and/or acceleration are measured along the pipe. The motions of the flexible pipe can be reconstructed through modal analysis. It is observed that the IL response frequency is often two times of the primary CF frequency ($1\times\omega$). In addition, higher harmonic components can also be present. In CF direction, third order harmonics ($3\times\omega$) are normally observed, as illustrated in Figure 1. Significant higher harmonics have been observed in VIV field tests [6]. The stress induced by the higher harmonics is significantly larger than that at the primary frequency. In many cases, the highest third order harmonic stress can be a factor of 1.6 of the stress at the primary shedding frequency. However, much smaller higher harmonics are also observed in other tests [5].

In order to obtain the hydrodynamic forces of a circular cylinder undergoing VIV, experiments on rigid cylinders are often performed. Gopalkrishnan [8] performed pure CF VIV forced motion tests on a rigid cylinder at Reynolds number of 10^4. Aronsen [9] carried out pure IL VIV forced motion tests on a rigid cylinder at Reynolds number of 2.4×10^4. He also performed combined IL and CF forced motion tests, and discovered that when there was IL motion, third order harmonics present in CF direction. Dahl [10] conducted an experimental study of the free vibration of an elastically mounted, rigid cylinder in a uniform flow, where the cylinder could move in both IL and CF directions. The natural frequency in each direction was tuned independently, allowing for an adjustment of the frequency ratio between IL and CF natural frequencies. The third order harmonic forces are more pronounced when the motion orbit of the cylinder is close to 'figure 8' shape and cylinder is moving against the flow at its largest CF motion. This study shows that significant third order harmonic forces are related to the cylinder motion orbits and reduced velocity. Later, Zheng [11] assessed the significance of higher order harmonics, confirmed Aronsen's finding – IL motion triggers the third order harmonics in CF direction. Zheng [11] carried out a large number of combined IL and CF forced motion VIV tests, building up a 2D VIV hydrodynamic coefficients database. Yin [12] carried out forced motion tests on a rigid pipe with measured orbits from NDP high mode VIV tests [1] and higher harmonics in both motions and forces were investigated. Bourget [13] and Wu [14] have shown that the orbits inside the excitation region of a flexible pipe are dominated by orbits which are moving against the flow at its largest CF motion.

Empirical VIV prediction programs, such as VIVANA [15], Shear7 [16] and VIVA [17], are widely used by the offshore industry. These programs rely on hydrodynamic force coefficient database to predict VIV responses. Such a database is normally generalized from measured force coefficients as a function of displacement amplitude ratio and non-dimensional frequency in 2D motion test with a rigid cylinder. Therefore, VIV response and the fatigue damage at the primary shedding frequency can be calculated. Modarres-Sadeghi et al. [18] constructed a higher harmonic hydrodynamic force coefficient database using combined CF and IL motion test data. By giving the flow velocity, cross-flow amplitude, in-line amplitude and phase difference as inputs to this database, the higher harmonic force components along the length of a flexible cylinder can be interpolated. This model seems to give reasonable prediction compared to the NDP high mode VIV test [1]. Jhingran and Vandiver [19] applied method to account 3rd order harmonic stress as a broad-banded Gaussian process in fatigue calculation. Wu et al. [20] used dual narrow-banded approach to calculate the fatigue damage when the responses at the primary ($1\times\omega$) frequency and 3rd order ($3\times\omega$) frequency can be approximated as two independent narrow-banded process.

Despite all these efforts, the influence of the key parameters on the occurrence and the magnitude of the third order harmonic stress is not well understood. A higher safety factor must be applied in VIV fatigue calculation to account for the additional contribution from the higher harmonics.

A reliable method to predict the third order harmonic stress is needed. It is desirable to obtain the magnitude of the third order harmonic stress directly from an empirical response model given the hydrodynamic and structural parameters. In this paper, the bending stiffness of the structure, the stationarity of the response travelling wave speed, motion orbits and the frequency contents of the responses along the pipe are systematically studied from an extensive set of VIV test data with flexible pipes. The objective is to identify the key parameters that lead to a significant third order harmonic stress and assess the importance of each one. A empirical response model that estimates higher harmonic stresses is proposed.

2 METHODOLOGY

Representative VIV test data of various flexible pipe models subjected to sheared flow profiles are studied, including NDP high mode VIV test [1], the Shell 38 m VIV test [2], the ExxonMobil rotating rig test [3],[4] and the Hanøytangen test [5]. Additional publicly available data from the MIAMI II tests [6] are also included. Selected cases with different towing speeds, response modes and time windows are summarized in Table 1. The theoretical background and the data analysis method are explained in this section. Bending stiffness, motion orbits and the frequency contents of the responses along the test models are extracted from these selected experimental data. Their influence on the third order harmonic stress is systematically studied and summarized in Section 3.

2.1 Theoretical background

The stiffness of a flexible pipe model in VIV tests normally has contributions from tension and bending stiffness. The natural frequencies of a tensioned beam are given by the following equations:

For a tensioned string:

$$f_{n,s} = \frac{\mathrm{n}}{2\mathrm{L}}\sqrt{\frac{T}{m}} \quad (1)$$

For an un-tensioned beam:

$$f_{n,b} = \frac{\mathrm{n}^2\pi}{2\mathrm{L}^2}\sqrt{\frac{EI}{m}} \quad (2)$$

For a tensioned beam:

$$f_{n,tot} = \sqrt{{f_{n,s}}^2 + {f_{n,b}}^2} \quad (3)$$

The calculated natural frequencies for the test models in present study are presented in Appendix A. The relative magnitude of the bending stiffness can be quantified by $f_{n,b}/f_{n,tot}$.

The theoretical wave travelling speed of an infinitely long tensioned string and a beam is calculated by the following equations:

Tensioned string:

$$C_s = \sqrt{\frac{T}{m}} \quad (4)$$

Un-tensioned beam:

$$C_b = \sqrt[4]{\frac{\omega^2\, EI}{m}} \quad (5)$$

For a tension-dominated string, the travelling speeds will be independent of the response frequency. This means that of the responses in IL and CF direction are the same. For a bending stiffness controlled beam, the longitudinal travelling speed depends on the response frequency. This means the primary CF response will be travelling along the pipe with a different speed that the IL response and higher order response must travel with higher speed than the primary one. It is hypothesized that the significance of the higher harmonics for a flexible pipe is also influenced by the bending stiffness of the structure, which can lead to different travelling speed of VIV response in

IL and CF directions. For a tension-dominated pipe, the travelling speeds of the responses in IL and CF direction are the same, which can lead to a long region with phase locked orbits [7].

Motion orbits may vary both in time and along the flexible pipe. In order to estimate the motion phase angle, it is assumed that the motion signal of a cross section can be represented by

$$y = Ycos(\omega t) \quad 6$$

$$x = Xcos(2\omega t + \theta) \quad 7$$

where x and y are the IL and CF displacements respectively.

The time difference Δt between the CF displacement zero up-crossing and the following IL displacement zero up-crossing is found. The phase difference θ between IL and CF is obtained by multiplying the time difference with the IL oscillation frequency:

$$\theta = 2\omega\Delta t - \frac{\pi}{2} \quad 8$$

Figure 2 presents an example of the various orbits to demonstrate the orbits with different phase angle θ. The orbits with phase angle smaller than 180 degrees move against the flow at the maximum CF response amplitude.

The displacement time series at the accelerator sensor locations can be obtained by integrating the acceleration signals twice. It can also be reconstructed by modal analysis techniques using strain and/or acceleration measurements. The time-varying CF or IL displacement along the pipe may be expressed as a sum of eigenmodes, or eigenfunctions:

$$x(z,t) = \sum_{n=1}^{\infty} w_n(t)\varphi_n(z), \quad z \in [0, L] \quad 9$$

where t is the time, z is the position along the pipe, L is the length of the pipe, $y(z,t)$ is the CF displacement of the pipe. Correspondingly, $x(z,t)$ the IL displacement of the pipe can be expressed similarly. $w_n(t)$ are the model weights, and $\varphi_n(z)$ are the mode-shapes, $n = 1, 2, 3, \ldots$.

The curvature is the second derivative of the displacement over riser length.

$$\kappa(z,t) = \sum_{n=1}^{\infty} w_n(t)\varphi_n''(z) \quad 10$$

where we can see that the phase angles between the IL and CF curvature will be the same as the displacement phase angles. The curvature can also be expressed from strain.

$$\kappa = \frac{\varepsilon}{R} \quad (11)$$

where ε is the strain, R is the riser outer radius where the strain gauges are located.

The motion phase angle can be calculated at each sensor location directly from the curvature signals. The phase between IL and CF curvature is calculated following the method mentioned above. IL and CF curvature amplitudes will not be directly comparable to the corresponding displacement amplitudes. However, the curvature phase angles will be the same as the displacement phase angles, and can therefore be used to construct 'orbits' of curvature in the same way as real orbits from displacements. Note that the relative values for IL and CF components for these 'orbits' will not represent the correct scaling of displacements. The CF and IL displacement/curvature time series are subdivided into sub-intervals. Each interval starts from one CF up-crossing point to the next, which corresponds to two periods of IL oscillation.

2.2 Wave travelling speed along a flexible pipe

In this section, we will discuss the expected travelling speed of actual riser model. As discussed in Equation 1, the bending stiffness has an increasing influence on the travelling speed with higher modes. The influence of the bending stiffness on the natural frequency is shown in Appendix A. The natural frequency of the first 32 modes of the Shell test pipe 2 is dominated by tension, which means that the travelling speed in IL and CF direction is expected to be close.

The measured signals have been bandpass filtered around CF (0.5×ω – 1.5×ω) and IL (1.5×ω – 2.5×ω) frequencies in the traveling speed and orbit phase angle estimation. The travelling speed of the response can be estimated by using contour plots of measured signals. The curvatures of CF (1×ω) and IL (2×ω) frequencies from Shell 38m test 3119 are plotted both in time and along the pipe in Figure 3. The response is selected from a stationary time window, where both response frequency and amplitude are stable. The travelling wave can be seen clearly, indicated by the thick dashed black line with arrow. The slope of this line gives the travelling speed. It can be seen that the travelling speed in both IL and CF directions are approximately the same. In this case, the CF response frequency is 9.8 Hz corresponding to mode 12, refer to Figure 12. IL frequency and mode are about twice of the CF one. As shown in Figure 12, the stiffness of the structure is tension controlled. Therefore, the wave travelling speeds in IL and CF directions are about the same according to Equation 4. The ratio between maximum stress at 3×ω and 1×ω frequency is 0.7. The NDP tests are found to give the same trends as the Shell experiments.

Figure 16 presents the natural frequencies of the riser model used in the ExxonMobil tests. In this set-up, the tension dominates the stiffness up to about 7th mode. The measured strain at CF (1×ω) and IL (2×ω) frequencies from ExxonMobil test 1218 are plotted both

in time and along the pipe in Figure 4. Note that the highest flow speed is at the bottom end of the pipe due to the test setup. Mixed travelling and standing waves are observed in the CF direction, but there are no clear travelling waves in the IL direction. CF frequency is about 8.8 Hz, which corresponds to mode 5. IL frequency is about twice of the CF frequency and IL response is about mode 8. As seen from Figure 16, the bending stiffness contribute significantly to the stiffness. The difference in travelling speed between IL and CF direction is calculated using Equations 4 and 5. However, it is difficult to estimate the IL travelling speed from Figure 4. The ratio between maximum stress at 3×ω and 1×ω frequency is 0.08. Also for the Hanøytangen test, the bending stiffness has large influence on the stiffness for the highest responding mode (>27), refer to Figure 13. IL and CF travelling speeds are about the same, at lower response modes (CF mode <12). IL response became chaotic with increasing mode number and no organized travelling wave patterns can be observed. IL wave travelling speed can not be estimated. At the highest flow speed cases, very high modes were observed especially in the IL direction (IL response mode >50). In the Miami test, the stiffness of the pipe is dominated by the tension as shown in Figure 14.

2.3 Motion Orbits in Travelling and Standing Wave Responses

The curvature orbits, motion phase angle and the curvature standard deviation values from Shell test case 3119 are presented in Figure 5. In Figure 5 (a), the curvature at each measurement location is given. For each orbit, the vertical direction is the CF direction and the horizontal direction is the IL direction. The motion phase angle is presented in the plot Figure 5 (b). The error bar indicates that variation of the phase angle (orbits shape) at different locations along the length of the pipe. Note that some of the variation is due to the round-off at 360 deg. In this plot, the motion phase angle shows a linearly increasing trend especially at the mid span of the pipe. This is mainly due to the presence of the strong travelling waves and the variation of reduced velocity [14]. The red line in the phase angle plot indicates a motion phase of 180 deg. The orbit directions are against the incoming flow at the largest CF amplitude if the motion phase angle is smaller than 180 deg. Orbits which have phase angle around 180 deg are shown to lead to significant high harmonic forces [10]. The ratio between the curvature standard deviation value at 3×ω frequency components and the maximum value of the 1×ω component is also presented in Figure 5 (c). It is seen in the plot that a significant 3×ω component (ratio > 0.4) occurs within the reduced velocity range Ur from 4 to 7. The highest 3×ω curvature ratio (≈ 0.7) has motion phase angles in the range of 135 - 180 deg.

Responses of the Shell test 3102 are presented in Figure 6. In this case, CF response is at 4^{th} mode, refer to . Strong standing waves are present due to the reflection at the boundary. The motion phase angle in the middle row of the figure shows zig-zag variation due to the presence of the standing waves. This is very different than the case where travelling wave is dominating the response, refer to Figure 5. It is difficult to have a long region of favorable motion orbits in this case. Therefore, the 3×ω curvature will be smaller. The ratio

between maximum stress at 3×ω and 1×ω frequency is 0.6 in this case. It is noted that the highest curvature ratio is found close to the low speed end in this case. However, the magnitude of the 3×ω curvature is also lower in this region. The highest curvature ratio is about 0.5 in the Ur range of 4 – 7.

2.4 Stability of the response

It has been observed that the VIV response can often switch from stationary to chaotic and vice versa. Wavelet analysis is applied in this study to reveal the frequency variation in time at selected locations along a riser. One such example is shown as the plot in the right-column in Figure 7, where the mid-column presents the corresponding curvature time series, and the left column shows the strain sensor location. It can be seen that there are two time-windows, i.e. 47 - 49 s and 50 - 52 s, where the response shows completely different behaviors. The response is chaotic in the time window from 47 - 49 sec. The envelope of the response amplitude has a strong variation and the response frequency shifts in time. There are no significant higher harmonics. This is due to the fact that orbits at one cross-section vary continuously in time, which may prevent the sustainable energy input that is needed to maintain the presence of significant higher harmonics. However, the response becomes rather stable in the next time window from 50 - 52 s. A strong frequency component at 3×ω is clearly seen, see Figure 5.

The orbits and motion phase angles from this chaotic response time window (47 - 49 s) are presented in Figure 8. They vary significantly in time, which is different from a stationary time window of the same test, see to Figure 5. The stress standard deviation at 3×ω frequency component is less than 20% of the maximum stress standard deviation at the primary shedding frequency. The same results are found in other cases where the response is chaotic.

3 SIGNIFICANCE OF THE THIRD ORDER HARMONIC STRESS

A significant 3×ω frequency component is observed in the Shell and NDP tests with a low response mode (CF mode <10). At low modes, the VIV response is often stationary and shows a mixture of travelling and standing waves behavior, which is caused by reflected waves from the boundaries. The stiffness of the structure is dominated by the tension. The standard deviation of the highest curvature at 3×ω frequency component is about 80% of the highest curvature at the primary shedding frequency.

With increasing CF response modes (10 - 15), the response can switch from stationary to chaotic and vice versa. Significant 3×ω frequency components are found in stationary response time windows. The orbits are stable in such cases. The highest 3×ω response occurs close to the middle-span of the models with corresponding reduced velocity 4<Ur<7, if the response is dominated by travelling waves. The motion phase angle is between 135 deg and 180 deg in this region. The CF and IL travelling wave speeds are about the same

as for a tensioned string. The standard deviation of the highest curvature at 3×ω frequency component can reach 80% of the highest curvature at the primary shedding frequency. In the chaotic response time window, no significant 3×ω frequency component is found. The motion orbits vary strongly in time. The standard deviation of the highest curvature at the 3×ω frequency component reduces to about 20% of the highest curvature at the primary shedding frequency.

The test pipe in the ExxonMobil rotating rig test has significantly higher bending stiffness compared to the Shell and NDP test pipes, refer to Table 2. The 3×ω frequency component is smaller than 20% of the highest curvature at the primary shedding frequency even at lower response mode.

The VIV response becomes completely chaotic for higher CF modes (>15) in the Hanøytangen test. The response frequency and envelope of the response amplitude vary in time. No significant 3×ω frequency component is found. The bending stiffness has significant influence on the total stiffness of the system. It is, however, difficult to estimate the wave propagation speed due to the relative low sensor density and chaotic response for such cases.

Significant higher harmonics were also observed from MIAMI II test [7]. The VIV responses in these cases are dominated by travelling waves. The Strouhal frequency $f_{St}(z) = S_t \frac{U(z)}{D}$ depends on the local flow speed. The dominant response frequency can be roughly estimated by using 80% of the highest flow speed. The corresponding mode number can be found assuming its natural frequency equals the estimated dominant response frequency. The natural frequency of the MIAMI II test pipe is presented in Figure 14. The dominating CF mode in MIAMI II test is typically higher than 25. The stress ratio of 3× ω/1× ω is about 1.0 - 1.5 with a mean value of 1.25 [6]. This ratio is 1.37 and 1.61 for two cases when a stationary time window is selected.

Based on these discussions, it is concluded that the relative magnitude of the 3× ω stress is influenced more by the bending stiffness than the mode number. The spatial maximum value of the standard deviation of the stress at 3×ω frequency component along the pipe is found for each analyzed case. Figure 9 plots the 3×ω/1×ω stress ratio as a function of the relative bending stiffness contribution. It shows that 3×ω stress is strongly related to the bending stiffness of the structure. Note that the location of the highest 3×ω stress often does not coincide with the location of the highest 1×ω stress.

A set of representative cases are selected to be further categorized in Figur**e 10**. It appears that significant higher harmonic stress components only occur when these conditions are simultaneously satisfied:

1) the riser has low bending stiffness contribution;

2) the riser response is stationary

3) the riser response is dominated by travelling waves.

It can be seen that this stress ratio is significantly higher (>1.0) when bending stiffness contribution is low (<0.35) except for cases dominated by the standing waves. A stress ratio >1.0 means that the stress amplitude for the 3×ω component is higher than for the primary frequency component. This may be due to the fact that this is a favorable condition for maintaining the phase lock when travelling speeds in CF and IL directions are close.

The stress ratio will be low (<0.4) when the response is chaotic and the shape of the motion orbits is varying constantly in time. The wave travelling speed for cases with higher bending stiffness contribution (>0.55) can have large difference in CF and IL directions, which will also be difficult for sustaining desired motion orbits.

The stress ratio is in general smaller than 0.8 when the response has a significant contribution from standing waves at lower response modes (<6). It must be noted that the spatial distribution of the motion orbits of these cases is significantly different. A zig-zag spatial distribution of the motion phase angle is observed. This means that the motion orbits or the phase angle difference can be large at two neighboring locations. Therefore, there will be alternating zones to support or suppress higher harmonics inside the excitation region. This may be less favorable for sustaining higher harmonics compared to a more gradual motion phase variation observed in a travelling wave dominated case, refer to Figure 5.

4 A PRELIMINARY HIGHER HARMONIC STRESS RESPONSE MODEL

It has been demonstrated that many parameters can influence the higher harmonic stress. It is desirable to be able to construct a response model to estimate the higher harmonic stress based on several key structural and hydrodynamic parameters, i.e., stationarity, bending stiffness contribution and travelling wave condition. Whether or when the response will be stationary may be difficult to predict. However, travelling wave response and bending stiffness contribution can be relatively easy to estimate.

A preliminary response model is proposed. Figure 11 is an envelope of the 3× ω/1× ω bending stress ratio based on all the experimental data. The highest 3×ω stress ratio is 1.6 when the relative bending stiffness ratio is smaller than 0.3. This ratio reduces to 0.4 with increasing bending stiffness.

It is shown that 3×ω stress ratio can be significantly lower (<0.8) even at low bending stiffness ratio if the standing wave dominates the response. Use of a stress ratio of 1.6 will be over-conservative in this case. A parameter to characterize finite or infinite structural behavior is the wave propagation parameter nζ [21]. ζ is the nth modal damping ratio (including both structural and hydrodynamic damping).

- nζ <0.2: spatial attenuation is small and standing wave will dominate the response.
- 0.2< nζ <2.0: mixed standing and travelling wave response.

- $n\zeta > 2.0$: the structure behaves as an infinitely long string and the travelling wave behavior will be dominant.

It is noted that the damping parameter ($n\zeta$) includes the hydrodynamic damping, which depends on the excitation and damping coefficients that will be used. As an example, an estimation of $n\zeta$ is about 1.0 based on Shell test 3119 and 3124. The $3\times\omega$ stress ratio is about 0.7 as shown in the figure. The corresponding CF dominating mode is 12-14. It is expected that higher response mode will lead to higher wave propagation parameter value. The stress ratio will also be higher. By including more test data, a more robust response model to estimate higher harmonics could be formulated.

5 CONCLUSIONS

The present study investigated the factors that influence the occurrence of higher harmonics in riser VIV response. The main emphasis was on the $3\times\omega$ frequency component in CF direction by analyzing VIV experimental data.

Based on the present data, it seems that there need to be long regions of stable and favorable motion orbits inside the excitation region in order to get significant higher harmonic stresses. This requires the following conditions:

- Response dominated by travelling waves
- Low relative bending stiffness contribution
- Stationary response

A preliminary empirical response model to estimate the CF 3rd order harmonic stress ratio is developed based on various lab tests and field test on riser in sheared current. It indicates that the significance of the higher harmonic stress can be different based on the structural and hydrodynamic characteristics of the riser. However, this empirical response model needs further validation with more model test data before it can be applied in VIV prediction practice. Methods to incorporate the higher harmonic stress in the fatigue calculation are also needed for accurate predictions of the fatigue life of marine risers.

ACKNOWLEDGMENTS

The authors are grateful to the Norwegian Deepwater Program (NDP) Riser and Mooring Project for funding and permission to publish this work. The authors would also like to acknowledge Shell International Exploration and Production for providing access to the Shell 38m VIV test data. Vortex Induced Vibration Data Repository is deeply appreciated for providing access to the ExxonMobil VIV test data.

REFERENCES

[1] Trim, A. D., Braaten, H., Lie, H., & Tognarelli, M. A. (2005). Experimental investigation of vortex-induced vibration of long marine risers. Journal of Fluid and Structures (21), 335-361.

[2] Lie, H., Braaten, H., Jhingran, V.G., Sequeiros, O.E., Vandiver, K., Comprehensive riser VIV model tests in uniform and sheared flow, OMAE2012-84055, July 2012, Rio de Janeiro, Brazil.

[3] Tognarelli, M. A., Slocum, S., Frank, W., & Campbell, R. (2004). VIV response of a long flexible cylinder in uniform and linearly sheared currents. Houston, USA: Offshore Technology Conference, OTC16338.

[4] The VIV Data Repository Project (VIVDR). http://web.mit.edu/towtank/www/vivdr/about.html

[5] Huse, E., Kleiven, G., Nielsen, F.G., 1998. Large scale model testing of deep sea risers. In: Proceedings of the Offshore Technology Conference, Houston, Texas, OTC 8701.

[6] Jhingran, V., 2008. Drag Amplification and Fatigue Damage in Vortex-Induced Vibrations. PhD dissertation, Massachusetts Institute of Technology, Cambridge, MA, USA.

[7] Vandiver, JK., Jaiswal, V., Jhingran, V. Insights on vortex-induced, traveling waves on long risers, Journal of Fluids and Structures 25 (2009) 641–653.

[8] Gopalkrishnan, R. (1992) Vortex-Induced Forces on Oscillating Bluff Cylinders, PhD dissertation, Massachusetts Institute of Technology, Cambridge, MA, USA.

[9] Aronsen, K. H., (2007). An experimental investigation of in-line and combined in-line and cross-flow vortex induced 446 vibrations. Ph.D. thesis, Norwegian University of Science and Technology, Norway.

[10] Dahl, J.M. (2008) Vortex induced vibrations of a circular cylinder with combined in-line and cross-flow motions. PhD dissertation, Massachusetts Institute of Technology, Cambridge, MA, USA.

[11] Zheng, H., (2014). The influence of high harmonic force on fatigue life and its prediction via coupled in line - cross flow VIV modeling. PhD dissertation, Massachusetts Institute of Technology, Cambridge, MA, USA.

[12] Yin, D., (2013). An experimental investigation of in-line and combined in-line and cross-flow vortex induced vibrations. Ph.D. thesis, Norwegian University of Science and Technology, Norway.

[13] Bourguet, R., Karniadakis, G., & Traiantafyllou, M. (2011). Vortex-induced vibrations of a long flexible cylinder in shear flow. Journal of Fluid Mechanics, 677, 342-382. doi:10.1017/jfm.2011.90.

[14] Wu, J., Lie, H., Larsen, CM., Liapis, S. & Baarholm, R. (2016).Vortex-induced vibration of a flexible cylinder: Interaction of the in-line and cross-flow responses, Journal of Fluids and Structures, Volume 63, Pages 238-258.

[15] Larsen, C.M., Lie H, Passano E, Yttervik R, Wu J, Baarholm G. VIVANA - Theory Manual, Version 4.10.1. SINTEF Ocean; 2017.

[16] Vandiver, J. K., Li L. SHEAR7 V4.4 Program Theoretical Manual. Department of Ocean Engineering, Massaccusetts Institute of Technology; 2005.

[17] Triantafyllou, M., Triantafyllou, G., David Tein, Y. S., & Ambrose, B. D. (1999). Pragmatic riser VIV analysis. Houston, USA: Offshore Technology Conference.

[18] Modarres-Sadeghi, Y., Mukundan, H., Dahl, J.M., Hover, F.S. and Triantafyllou, M.S. (2010), The effect of hihger harmonic forces on fatigue life of marine risers, Journal of Sound and Vibration 329, 43-55.

[19] Jhingran, V., Vandiver, J.K., 2007. Incorporating the higher harmonics in VIV fatigue predictions. In: Proceedings of the 26th International Conference on Offshore Mechanics and Arctic Engineering, OMAE2007-29352.

[20] Wu, J., Yin, D.C., Lie, H., Larsen, C. M., Baarholm, R. J., Jhingran, V., and Liapis, S., On the occurrence of higher harmonics in the VIV response, Proceedings of Offshore Mechanics and Arctic Engineering Conference 2015, OMAE2015-42061, June 2015, St. John's, Newfoundland, Canada.

[21] Vandiver, J.K., Dimensionless parameters important to the prediction of vortex-induced vibration of long, flexible cylinders in ocean currents, Journal of Fluids and Structures, July 1993.

APPENDIX A

PIPE PROPERTIES AND NATURAL FREQUENCIES

List of Figures

List of Tables

Table 1 Overview of the analyzed cases.

Model Test	**Test No.**	**U_{max} [m/s]**	**$f_{CF,dom}$ [Hz]**	**$N_{CF,dom}$**
Shell 38 m	3102	0.47	2	4
	3103	0.57	2.4	6
	3105	0.47	3.1	9
	3119	2.55	9.8	12
	3124	2.73	10.1	~ 14
Hanøytangen	37	0.44	2.3	10
	39	0.64	2.8	12
	45	0.84	3.18	15
	56	1.36	6.2	22
	66	1.96	7.02	~ 27
Exxon Mobil rotating rig*	1201 - 1220	0.20 - 1.96	1.31 - 14.2	1 - 7
NDP high mode**	2310 - 2520	0.3 - 2.4	1.64 - 11.09	2 - 14
Miami II	20061023203818 20061023205043 20061023205557 20061023204504 20061022153003 20061022153702	~ 0.85 - ~ 1.34	~ 3.71 - ~ 5.85	~ 25 - ~ 39

*) All together 20 tests with increasing velocity from 0.2 m/s to 1.96 m/s

**) All together 22 tests with velocity increment of 0.1 m/s

Table 2 Physical properties of the test pipes

Parameter	Shell 38m (Pipe2)	Hanøytangen	MIAMI II	NDP High Mode	ExxonMobil
Total length between pinned ends (m)	38	90	152.4	38	9.63
Outer diameter (mm)	30	30	36.3	27	20
Bending stiffness, EI (Nm^2)	572.3	3640	613	572.3	135.4
Young modulus, E (N/m^2)	3.46×10^{10}	2.1×10^{11}	9.21×10^{9}	3.46×10^{10}	1.02×10^{11}
Mass in air (kg/m)	1.088	2.27	0.76	1.088	0.70
Mean Tension (N)	4000	3700	3225	4000	700

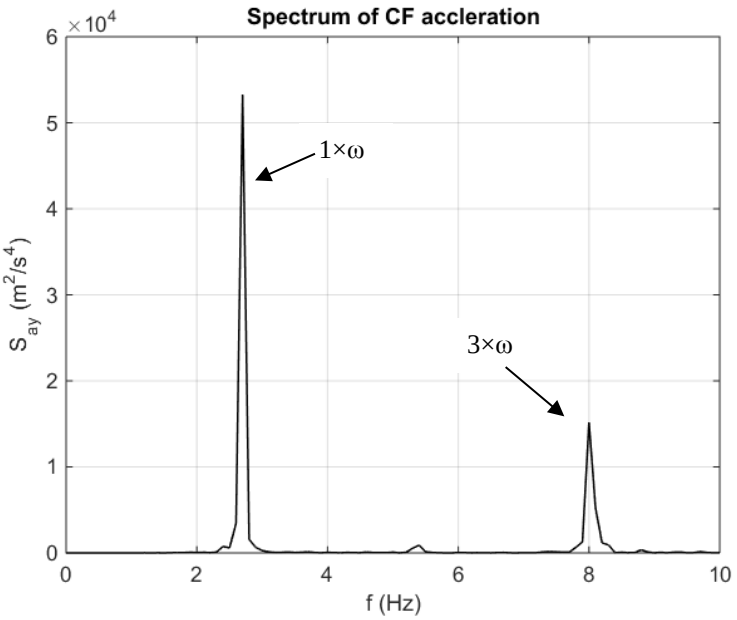

Figure 1 An example of the CF acceleration spectrum.

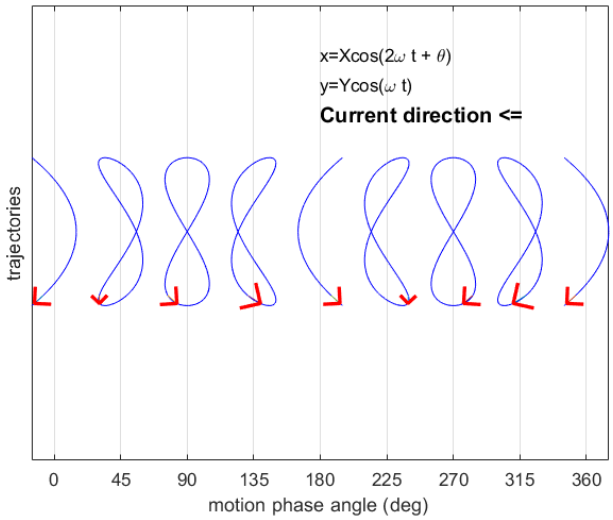

Figure 2 Typical motion orbits. The orbit direction is indicated by the direction of the red arrow. The flow is coming from right to left.

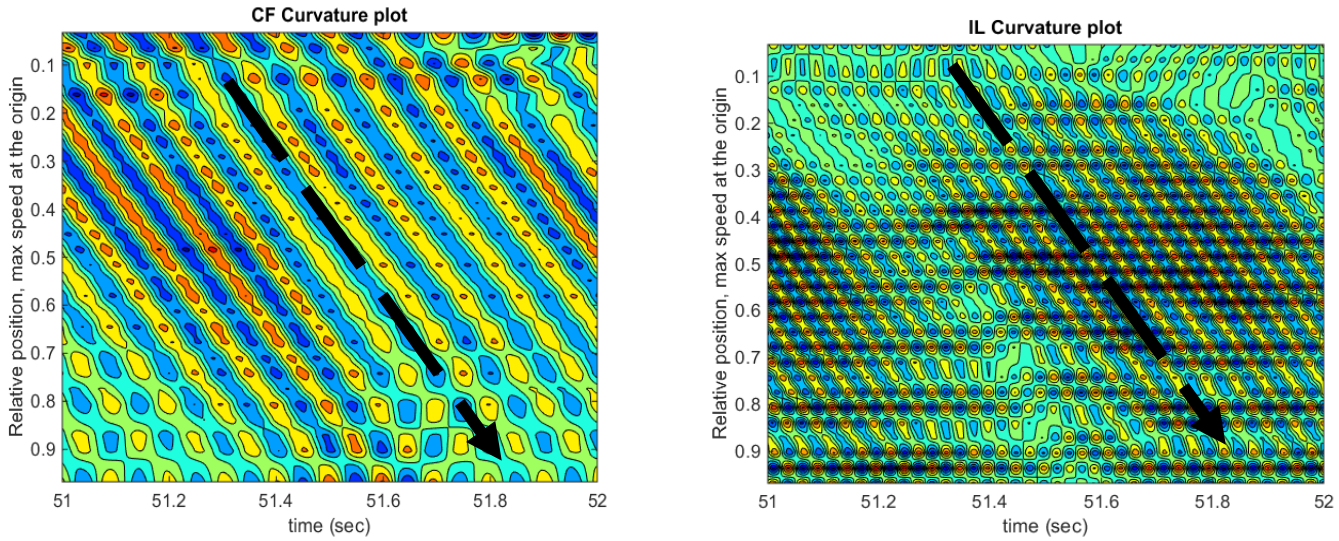

a

b

Figure 3 CF and IL curvature plot for Shell test 3119 (stationary response time window). Note the slope of the black line gives an estimate of the travelling speed.

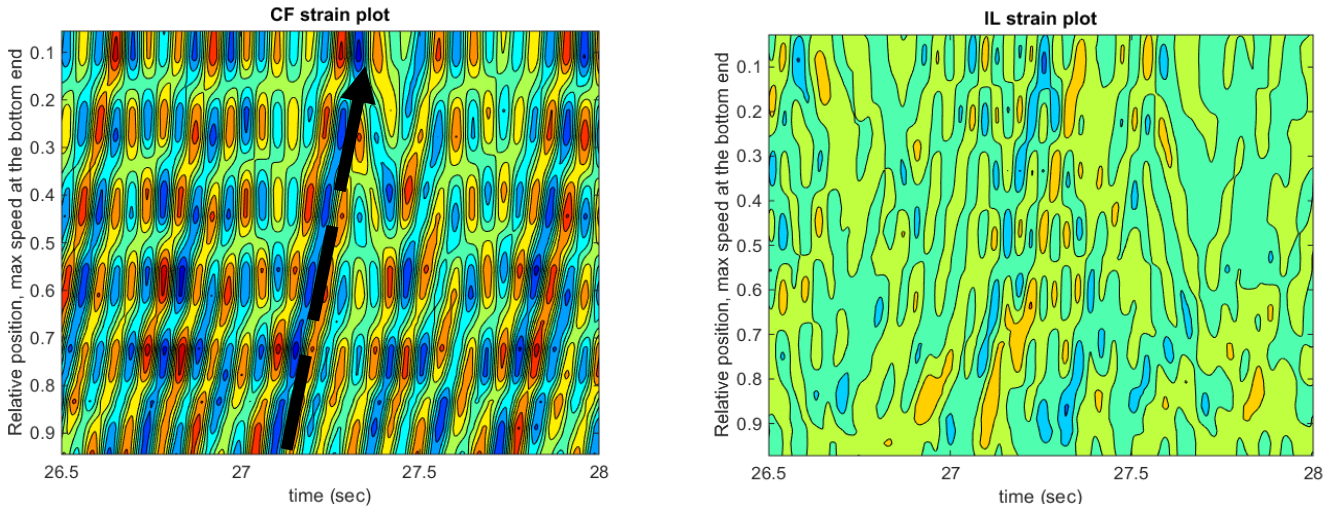

a b

Figure 4 CF and IL strain plot for ExxonMobil test 1218. No clear travelling waves are observed in the IL direction.

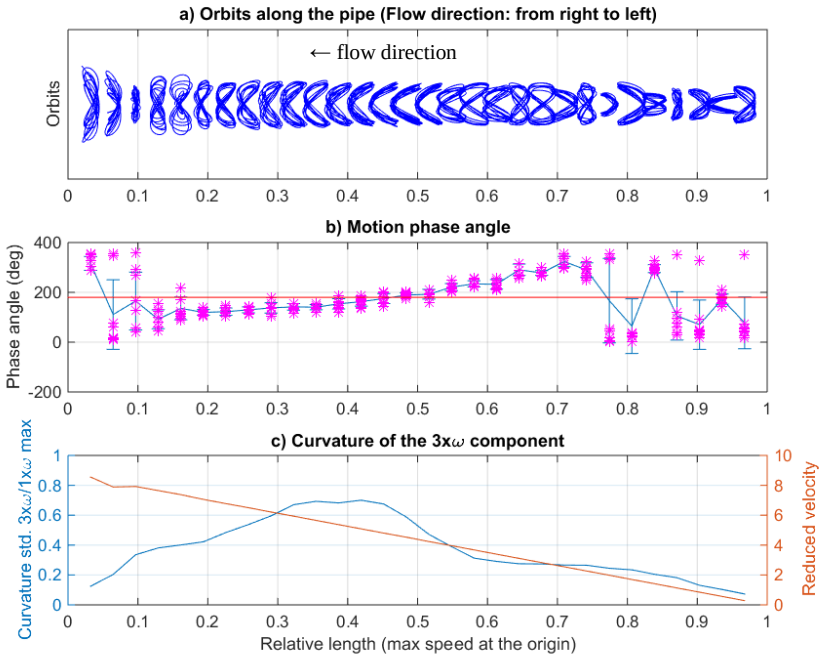

Figure 5 Example of traveling wave type response. Orbits, motion phase angle and curvature for Shell test 3119. Flow comes from right to left.

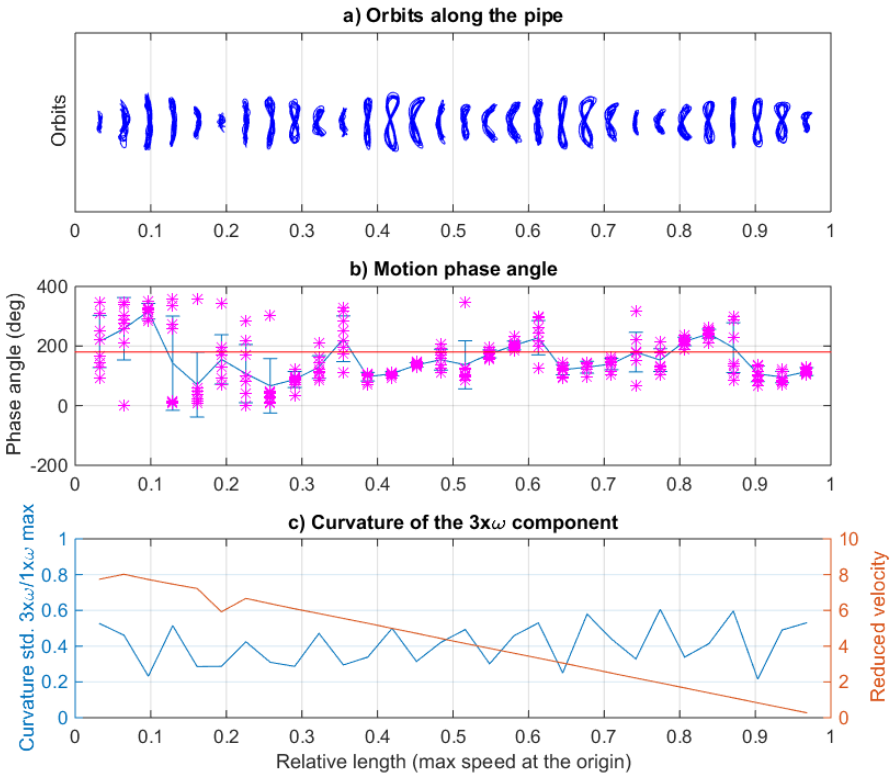

Figure 6 **Example of standing wave type response. Orbits, motion phase angle and curvature for the Shell test 3102. Flow comes from right to left.**

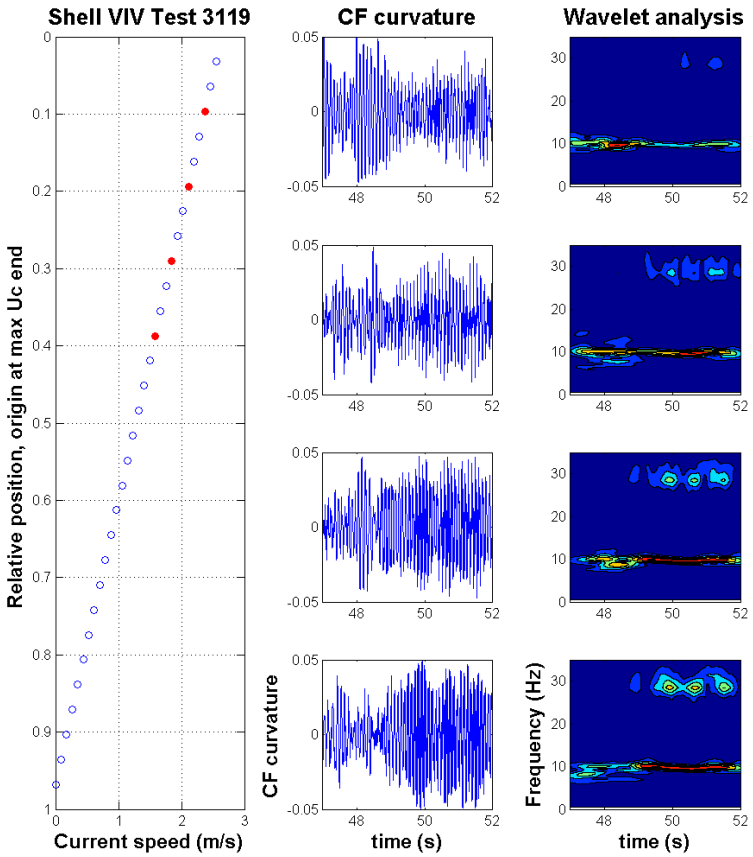

Figure 7 Response example when the first part of the time series are chaotic and the last become stationary. Wavelet analysis of selected curvature measurements for Shell test 3119. The flow speed profile at measurement location is shown in the first plot. Four measured curvature signals are selected to be analyzed. Their locations along the riser are marked by filled circles

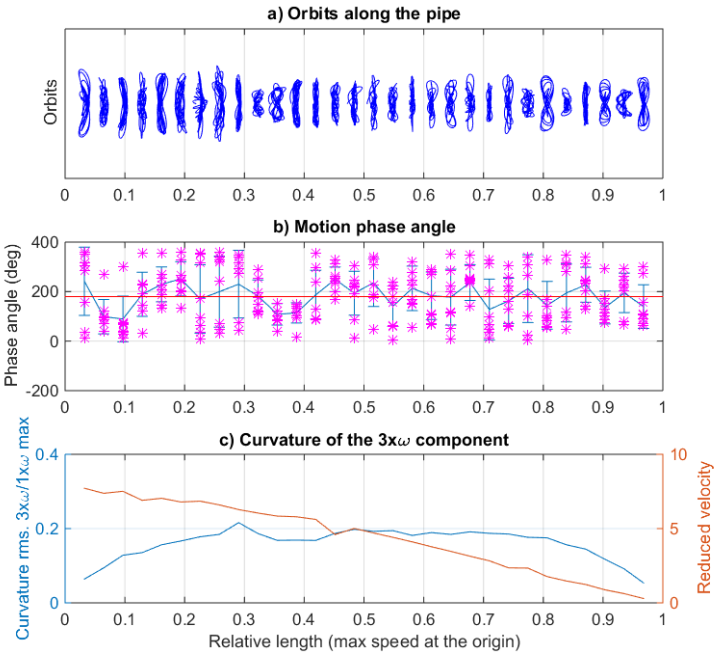

Figure 8 Example of chaotic response type. Orbits, motion phase angle and curvature for Shell test 3119 (chaotic response time window 47-49 sec). Flow comes from right to left.

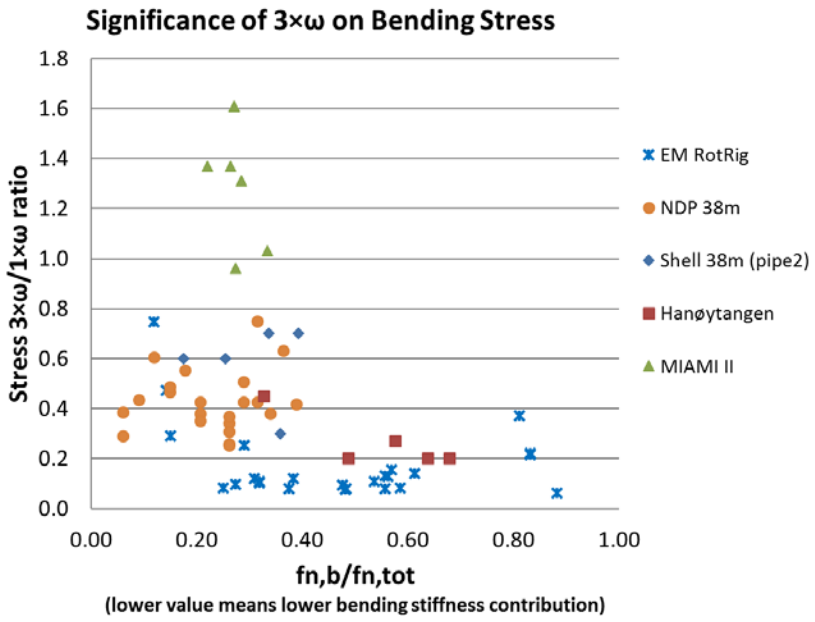

Figure 9 Maximum 3×ω/1×ω stress ratio vs. relative bending stiffness contribution

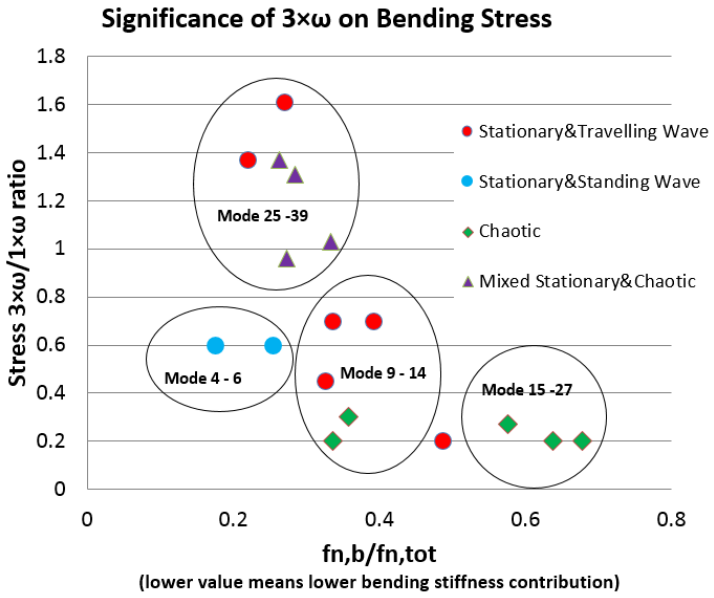

Figure 10 Influence of the bending stiffness on the significance of the 3×ω stress ratio of an flexible pipe subjected to sheared flow profiles. The color and shape of the symbols represent different response characteristics. The diamond symbol represents the chaotic response. The red circular symbol represents the stationary response dominated by travelling waves. The blue circular symbol represents the stationary response dominated by standing waves. The triangular symbol represents data taken from total time window, which may include both chaotic and stationary response time periods. The data has also been grouped in terms of CF mode order.

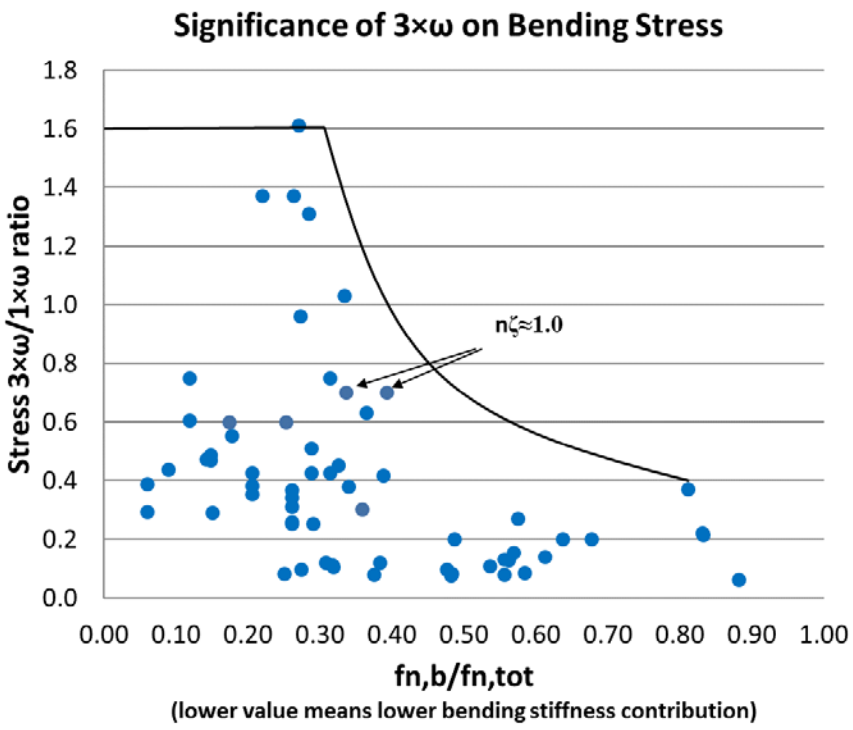

Figure 11 Preliminary empirical response model (black lines) to estimate 3× ω/1× ω bending stress ratio. The blue dots are the data points from Shell, NDP, ExxonMobil, Hanøytangen and MIAMI II tests.

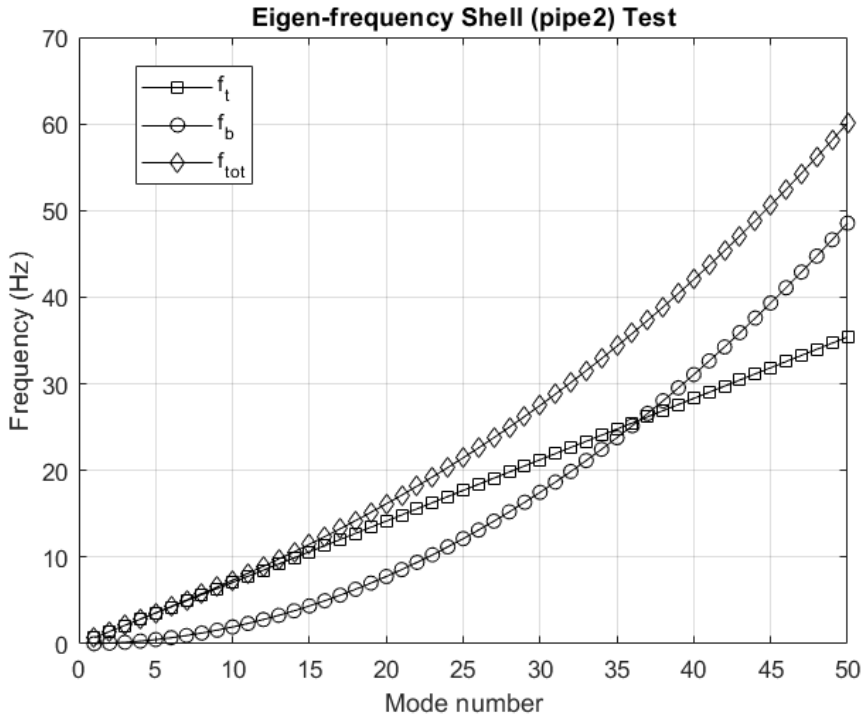

Figure 12 Eigen-frequencies of the Shell 38m test (pipe2). The squares represent the eigen-frequencies of a tensioned string; the circles represent the eigen-frequencies of a beam; and the diameters represent the actual eigen-frequencies of a tensioned beam. The mean tension is about 4000 N in this case.

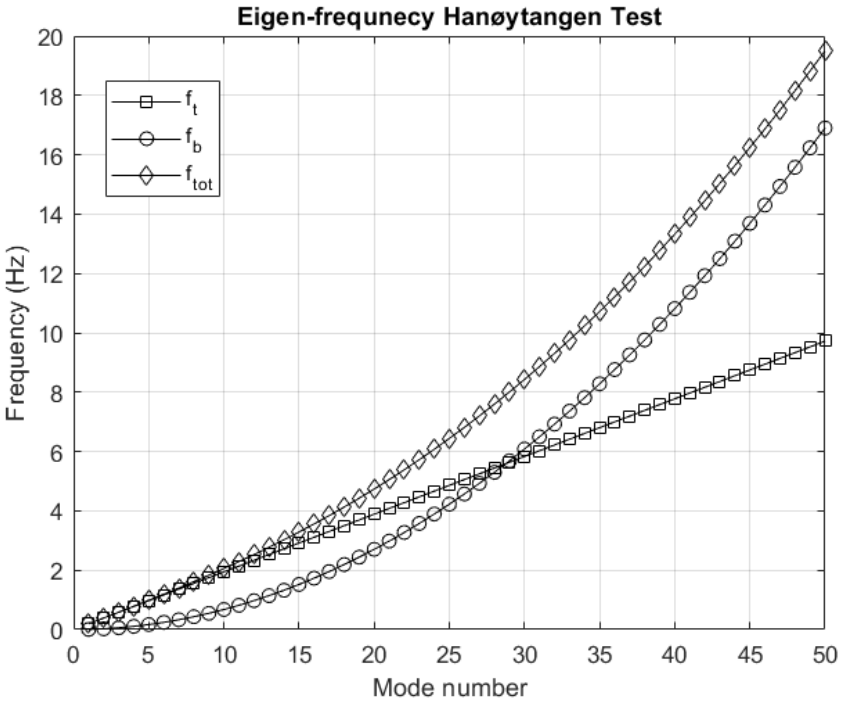

Figure 13 Eigen-frequencies of the Hanøytangen test pipe. The squares represent the eigen-frequencies of a tensioned string; the circles represent the eigen-frequencies of a beam; and the diameters represent the actual eigen-frequencies of a tensioned beam.

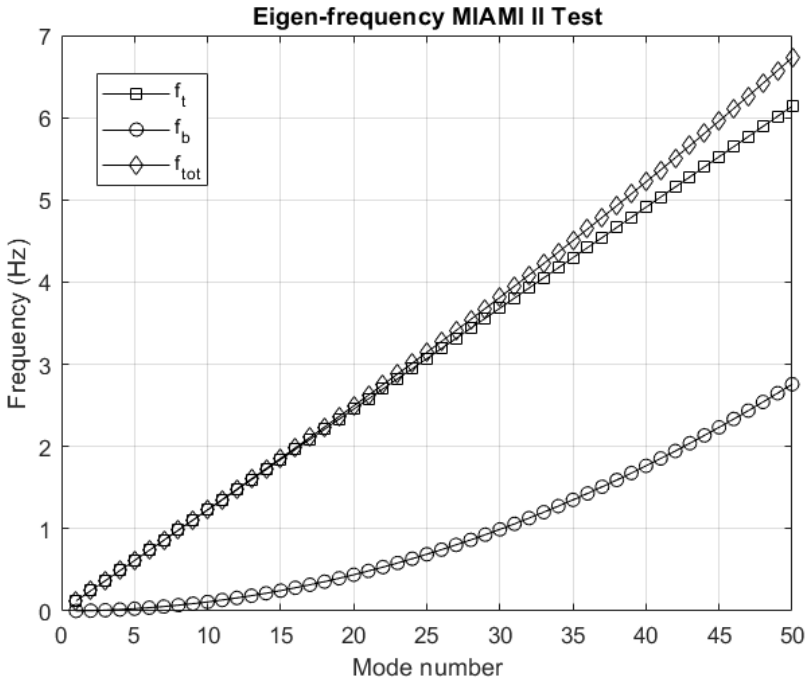

Figure 14 Eigen-frequencies of the MIAMI II test pipe. The squares represent the eigen-frequencies of a tensioned string; the circles represent the eigen-frequencies of a beam; and the diameters represent the actual eigen-frequencies of a tensioned beam.

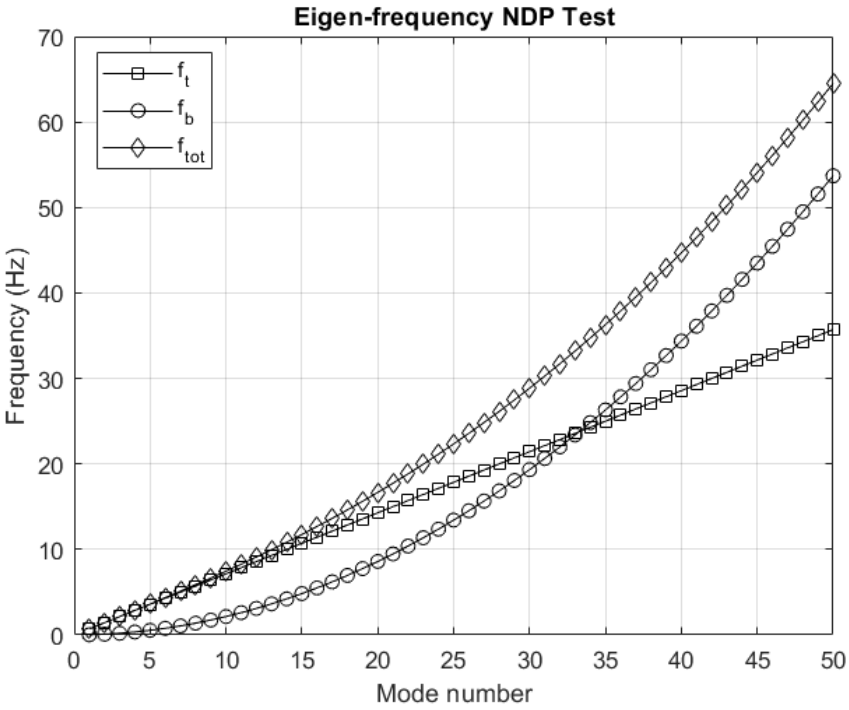

Figure 15 Eigen-frequencies of the NDP high mode VIV test pipe. The squares represent the eigen-frequencies of a tensioned string; the circles represent the eigen-frequencies of a beam; and the diameters represent the actual eigen-frequencies of a tensioned beam. The mean tension is about 4000 N in this case.

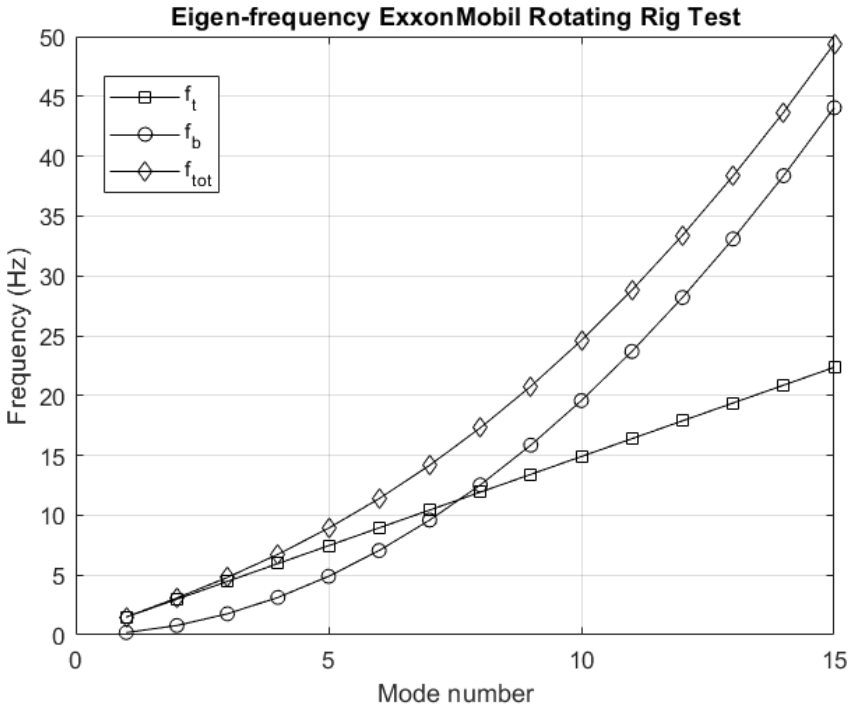

Figure 16 Eigen-frequencies of the ExxonMobil rotating rig test pipe. The squares represent the eigen-frequencies of a tensioned string; the circles represent the eigen-frequencies of a beam; and the diameters represent the actual eigen-frequencies of a tensioned beam. The mean tension is about 700 N in this case.